9. N. Ojaroudi and N. Ghadimi, Band-notched UWB slot antenna, Microwave Opt Technol Lett 56 (2014), 1744–1747.

10. N. Ojaroudi, Sh. Amiri, and F. Geran, Reconfigurable monopole antenna with controllable band-notched performance for UWB communications, In: 20th Telecommunications Forum, TELFOR 2012, November 20–22, 2012, Belgrade, Serbia, 2013, pp. 1176–1178.

11. J. William and R. Nakkeeran, CPW-Fed UWB slot antenna with reconfigurable rejection bands, In: Proceedings of International Conference on Control, Communication and Power Engineering, 2010.

12. S.L. Steven Yang, A.A. Kishk, and K.F. Lee, Frequency reconfigurable U-slot microstrip patch antenna, IEEE Antennas Wireless Propag Lett 7 (2008), 127–129.

13. Ansoft Corporation, Ansoft high frequency structure simulation (HFSS), Ver. 13, Ansoft Corporation, Pittsburgh, PA, 2010.

14. N. Ojaroudi, H. Ojaroudi, and N. Ghadimi, Quad-band planar inverted-f antenna (PIFA) for wireless communication systems, Prog Electromagn Res Lett 45 (2014), 51–56.

15. N. Ojaroudi, Microstrip monopole antenna with dual band-stop function for UWB applications, Microwave Opt Technol Lett 56 (2014), 818–822.

16. N. Ojaroudi, Circular microstrip antenna with dual band-stop performance for ultra-wideband systems, Microwave Opt Technol Lett 56 (2014), 2095–2098.

17. N. Ojaroudi and N. Ghadimi, Design of CPW-FED slot antenna for MIMO system applications, Microwave Opt Technol Lett 56 (2014), 1278–1281.

18. N. Ojaroudi and N. Ghadimi, Dual-band CPW-fed slot antenna for LTE and WiBro applications, Microwave Opt Technol Lett 56 (2014), 1013–1015.

19. Avago Technologies, HPND-4005, Beam lead PIN diode, Avago Technologies.

20. S. Nikolaou, N.D. Kingsley, G.E. Ponchak, J. Papapolymerou, and M.M. Tentzeris, UWB elliptical monopoles with a reconfigurable band notch using MEMS switches actuated without bias lines, IEEE Trans Antenna Propag 57 (2009), 2242–2251.

SMALL-SIZE DUAL-WIDEBAND MONOPOLE ANTENNA WITH INDUCTIVE AND CAPACITIVE FEEDING BRANCHES FOR LONG TERM EVOLUTION TABLET COMPUTER APPLICATION

Kin-Lu Wong and Zih-Guang Liao
Department of Electrical Engineering, National Sun Yat-sen University, Kaohsiung 80424, Taiwan; Corresponding author: wongkl@ema.ee.nsysu.edu.tw

ABSTRACT: *A small-size dual-wideband monopole antenna for the long term evolution (LTE) operation in the tablet computer is presented. The antenna occupies a small ground clearance of 10×30 mm^2 and is easy to implement by feeding a simple radiating portion through an inductive branch (inductor-loaded branch) and a capacitive branch (capacitor-loaded branch). The inductive branch mainly generates the antenna's lower band and leads to decreased resonant size for the antenna, while the capacitive branch is mainly for generating the antenna's higher band. By further aided by a simple matching network, both the antenna's lower and higher bands can have enhanced bandwidths. In this study, the antenna not only occupies a small ground clearance but also has a thin thickness of 3 mm only, and the obtained bandwidths can cover two wide bands of 698–960 and 1710–2690 MHz for the LTE operation. Details of the proposed antenna are presented.* © 2015 Wiley Periodicals, Inc. Microwave Opt Technol Lett 57:853–860, 2015; View this article online at wileyonlinelibrary.com. DOI 10.1002/mop.28956

1. INTRODUCTION

It has been shown that dual-band or dual-wideband operation of the mobile device antenna can be obtained based on applying the matching circuit design or the passive switching circuit design [1–4]. By applying such a design concept, the long term evolution (LTE) dual-wideband operation in the 698–960 and 1710–2690 MHz bands with a single feeding port [2, 3] or two feeding ports [3, 4] has been obtained for internal mobile device antennas. In these antennas, simple radiating portions can be applied, leading to a simple antenna configuration. As the dual-wideband operation is obtained mainly by the passive switching circuit design, these antennas are referred here as circuit-defined antennas. With the LTE dual-wideband operation obtained, the antenna volume can occupy a small size of $10 \times 30 \times 3.8$ mm^3 for the tablet computer [4] or a small size of $10 \times 50 \times 5$ mm^3 for the mobile handset [2, 3].

The dual-wideband technique of using the passive switching circuit design is different from the traditional design mainly based on configuring the antenna's radiating portion [5], which generally leads to a complicated antenna configuration and a larger antenna volume as well. Take the example of many reported LTE antennas for applications in the mobile device such as the tablet computer to cover the 698–960 and 1710–2690 MHz bands [6–16], very few of them can fit in a small ground clearance of less than 10×40 mm^2 inside the tablet computer, although their antenna structures are compactly configured. Conversely, the recently reported LTE tablet computer antenna based on the passive switching circuit design occupies a small ground clearance of 10×30 mm^2 only [4]. Hence, from the antenna's size and configuration considerations, the circuit-defined antenna for dual-wideband operation [2–4] is attractive for the LTE operation in modern mobile devices. However, the circuit design required in achieving the LTE dual-wideband operation in [2–4] is still relatively complicated. If the circuit design can be further simplified, such circuit-defined antennas will be more attractive for practical applications.

In this article, we present the design of a new circuit-defined antenna with two hybrid feeding branches and a simple matching network to achieve the LTE dual-wideband operation for the tablet device application. The antenna is a simple monopole with an inductive feeding branch and a capacitive feeding branch. The antenna can be disposed in a small ground clearance of 10×30 mm^2 in the tablet computer. Through the inductive and capacitive feeding branches, the antenna can generate resonant modes, respectively, in the desired lower and higher bands. In the inductive feeding branch, a proper chip inductor (7.0 nH in this study) is embedded to decrease the required resonant length of the antenna in the lower band, thereby effectively reducing the antenna size to fit in the small ground clearance in this study [17–19].

Conversely, owing to the large reactance of the embedded chip inductor at higher frequencies, higher-order resonant modes of the antenna's simple radiating portion cannot be excited in the desired higher band by the inductive feeding strip. It is found that by adding a capacitive feeding strip with a proper chip inductor (1.0 pF in this study) embedded therein, a path for feeding the antenna at frequencies in the desired higher band can be obtained, which causes a resonant mode excited in the desired higher band. Then, by further aided using a simple
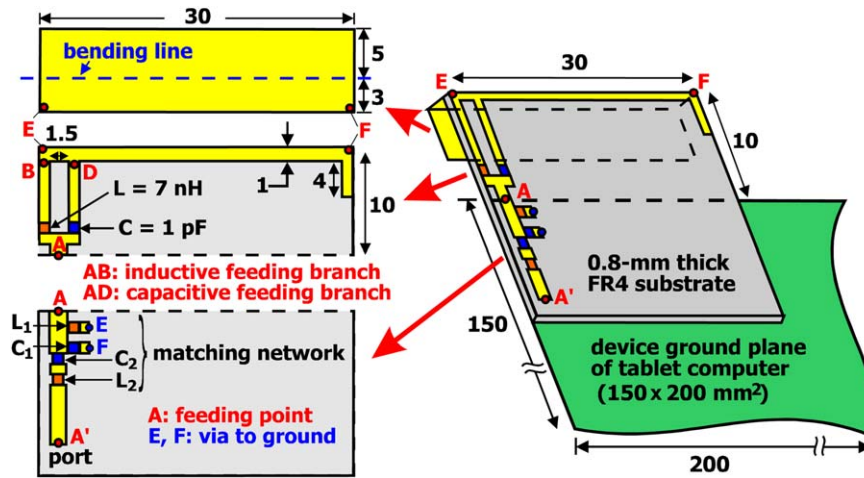
Figure 1 Geometry of the simple monopole antenna with inductive and capacitive feeding branches for the LTE/WWAN tablet computer. [Color figure can be viewed in the online issue, which is available at wileyonlinelibrary.com]

matching network, the operating bandwidths of the antenna's lower and higher bands can be greatly widened to cover the 698–960 and 1710–2690 MHz bands. Note that the matching network can be disposed on a small area of the system circuit board of the tablet computer, and it has been very common that there is a board space reserved for the matching network on the system circuit board of the handheld device [1–4, 20, 21].

In this study, the proposed antenna shows a novel antenna structure (a monopole with inductive and capacitive feeding branches) and a much simplified matching network than those applied in [2–4]. Furthermore, the antenna not only fits in the small ground clearance of 10×30 mm^2 but also has a thin thickness of 3 mm only, which is promising for modern slim tablet computer applications. Details of the proposed antenna and the obtained results are presented.

2. PROPOSED ANTENNA

Figure 1 shows the proposed simple monopole antenna with inductive and capacitive feeding branches for the LTE tablet computer. The antenna can provide two wide operating bands and occupies a clearance region of 10×30 mm^2 along the top edge of the ground plane of size 150×200 mm^2. The selected size of the device ground plane is for applications in a popular 9.7-in. tablet computer. The antenna comprises a printed metal pattern on a 0.8-mm thick FR4 substrate (relative permittivity

4.4 and loss tangent 0.024) and a metal plate bent into an L shape of size $3 \times 5 \times 30$ mm^3 and connected to the printed metal pattern. The printed metal pattern is mainly an inverted-F shape. It includes a 1-mm wide metal strip of length 34 mm, an inductive feeding branch (strip AB) loaded by a chip inductor of 7 nH (L), and a capacitive feeding branch (strip AD) loaded by a chip capacitor of 1 pF (C). The inductive feeding branch mainly controls the antenna to generate a resonant mode in the
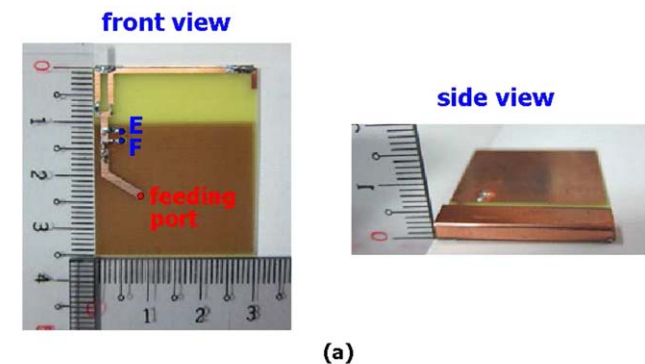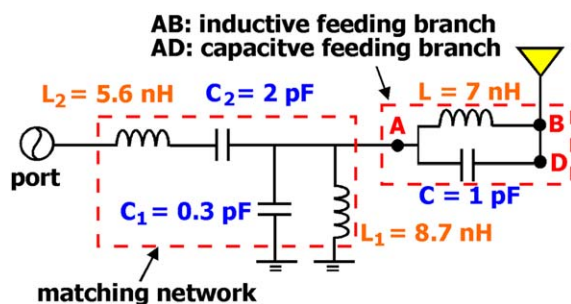

Figure 2 Equivalent circuit model of the matching network, the inductive feeding branch, and the capacitive feeding branch. [Color figure can be viewed in the online issue, which is available at wileyonlinelibrary.com]

Figure 3 Photos of (a) the fabricated antenna and (b) the antenna with the device ground plane. [Color figure can be viewed in the online issue, which is available at wileyonlinelibrary.com]
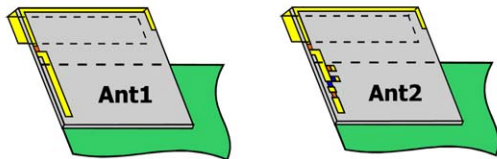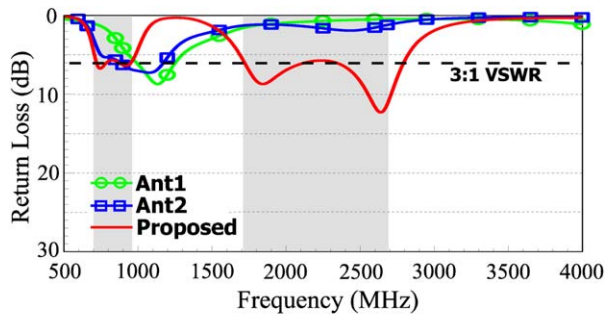
Figure 4 Simulated return loss for the proposed antenna, the case without the capacitive feeding branch and matching network (Ant1), and the case without the capacitive feeding branch (Ant2). [Color figure can be viewed in the online issue, which is available at wileyonlinelibrary. com]

Figure 5 Simulated return loss for the proposed antenna, the case without the inductive feeding branch and matching network (Ant3), and the case without the inductive feeding branch (Ant4). [Color figure can be viewed in the online issue, which is available at wileyonlinelibrary. com]

desired lower band, while the capacitive feeding branch leads to the generation of a resonant mode in the desired higher band.

A simple matching network consisting of a shunt chip inductor (L_1, 8.7 nH), a shunt chip capacitor (C_1, 0.3 pF), a series chip capacitor (C_2, 2 pF), and a series chip inductor (L_2, 5.6 nH) is disposed on the device ground plane. The equivalent circuit model of the matching network and the two feeding branches are shown in Figure 2. The matching network causes dual-resonance excitation of the excited resonant modes in the antenna's lower and higher bands to, respectively, cover the desired 698–960 and 1710–2690 MHz bands. The dual-resonance excitation in the lower band is mainly owing to the inductor L_1 and the capacitors C_1, C_2, while the dual-resonance excitation in the higher band is mainly owing to the inductor L_2. Detailed effects of the matching network will be discussed in the next section. Also, note that the short strip of length 4 mm at the open end of the printed metal strip is mainly used to slightly adjust the antenna's lower band to cover the desired 698–960 MHz band.

Figure 3(a) shows the photo of the fabricated antenna in its front and side views. In the experimental testing, the antenna is mounted to the top edge of the device ground plane as shown in Figure 3(b). Both the device ground plane and the L-shaped metal plate connected to the printed metal pattern are cut from a 0.2-mm thick copper plate in this study. In the experiment, a 50-Ω SMA connector is connected to the feeding port to feed the antenna. Detailed experimental results are presented in Figures 12–14 and will be discussed later.

3. OPERATING PRINCIPLE AND PARAMETRIC STUDY

3.1. Design Procedure
The first step in the proposed design starts from choosing the length of the simple printed strip (section EF) on the FR4 substrate to be 30 mm (0.25 wavelength at 2.5 GHz). The simple strip can support a resonant mode in the desired higher band. However, the excited resonant mode will have a bandwidth far less than 1 GHz to cover the LTE high band (1710–2690 MHz).
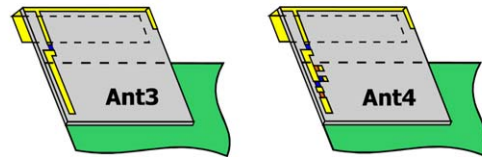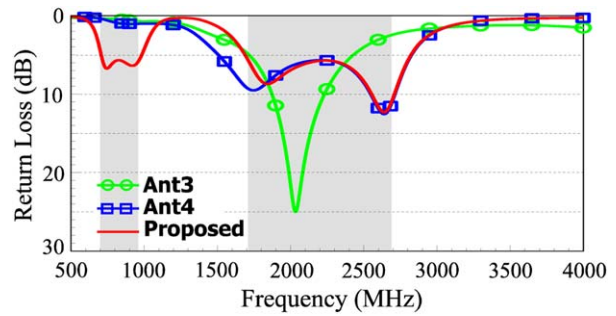
The second step is to add the inverted-L metal plate to section EF to increase the bandwidth of the excited resonant mode, although the widened high-band bandwidth will be still much less than 1 GHz.

The third step is to add the two hybrid feeding strips and select proper chip inductor and chip capacitor to be embedded in the two feeding strips. In this step, an additional resonant mode can be generated in the desired lower band, thus resulting in a dual-band operation for the antenna (see the results shown in Fig. 6, which will be discussed later).

The fourth step is to add the proposed matching network, which can greatly enhance the bandwidths of the antenna's lower and higher bands. This leads to a dual-wideband operation for the antenna to cover the 689–960 and 1710–2690 MHz bands for the LTE operation.

3.2. Operating Principle
Effects of the inductive feeding branch are first analyzed. Figure 4 shows the simulated return loss for the proposed antenna, the case without the capacitive feeding branch and matching network (Ant1) and the case without the capacitive feeding branch (Ant2). Corresponding parameters of the proposed antenna, Ant1, and Ant2 are the same. Two shaded frequency ranges are
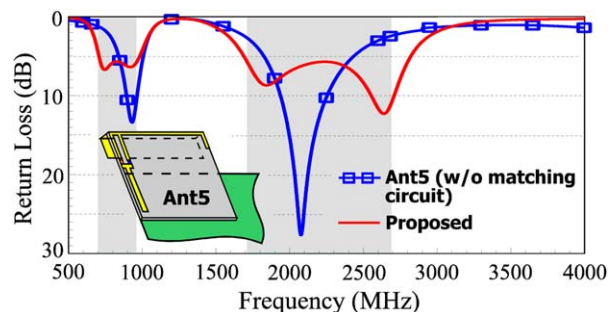

Figure 6 Simulated return loss for the proposed antenna and the case without the matching network (Ant5). [Color figure can be viewed in the online issue, which is available at wileyonlinelibrary.com]
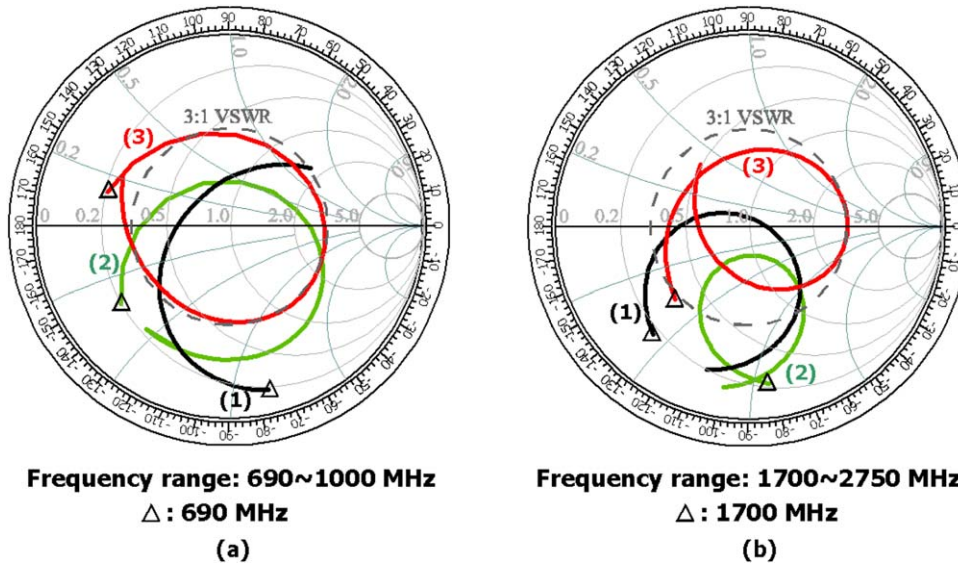
Figure 7 Simulated input impedance on the Smith chart for Ant5 (curve 1), Ant5 with L_1, C_1, C_2 (curve 2), and Ant5 with L_1, C_1, C_2, L_2 (curve 3, proposed antenna). (a) Frequency range: 690–1000 MHz. (b) Frequency range: 1700–2750 MHz. [Color figure can be viewed in the online issue, which is available at wileyonlinelibrary.com]
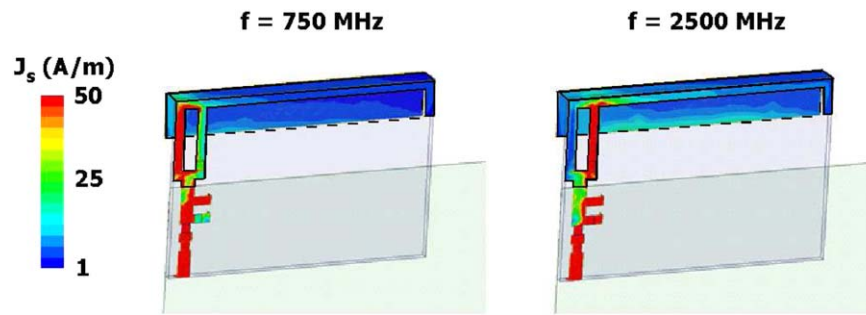

Figure 8 Simulated surface current distributions of the proposed antenna at 750 and 2500 MHz. [Color figure can be viewed in the online issue, which is available at wileyonlinelibrary.com]

the desired lower and higher bands. The simulated results are obtained using the HFSS version 15 [22]. It is seen that the desired higher band cannot be generated for Ant1 and Ant2. This is because the desired higher band is mainly generated owing to the capacitive feeding branch, which will be discussed later with the aid of Figure 5. Also, for Ant1, owing to the loaded inductance of $L = 7$ nH which decreases the antenna's

resonant length [17–19], a resonant mode is excited at about 1.15 GHz. Note that when a simple feeding strip is applied (that is, $L = 0$), the resonant mode occurs at about 1.45 GHz (not shown in the figure). By adding the matching network to form Ant2, the resonant mode is shifted to lower frequencies and a dual-resonance excitation also occurs to achieve a wider bandwidth. Also note that, for the proposed antenna, the simulated

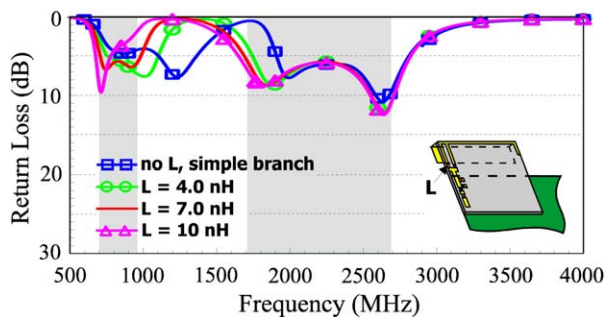**Figure 9** Simulated return loss as a function of the inductance L in the inductive feeding branch. [Color figure can be viewed in the online issue, which is available at wileyonlinelibrary.com]
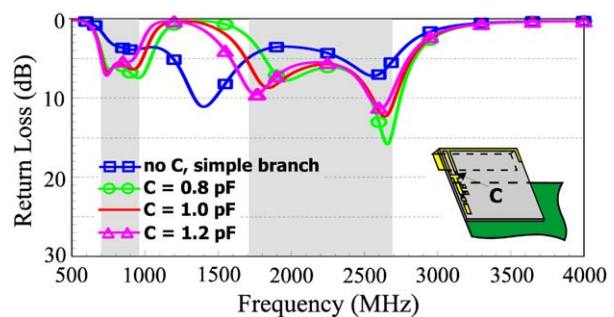

Figure 10 Simulated return loss as a function of the capacitance C in the capacitive feeding branch. [Color figure can be viewed in the online issue, which is available at wileyonlinelibrary.com]
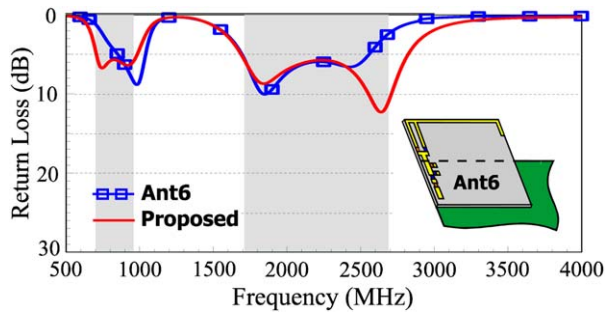
Figure 11 Simulated return loss for the proposed antenna and the case with a planar metal plate (Ant6). [Color figure can be viewed in the online issue, which is available at wileyonlinelibrary.com]

return loss is generally better than 6 dB in the desired lower and higher bands (see two shaded frequency ranges in the figure), except for some frequencies slightly less than 6 dB. The simulated and measured antenna efficiency is all better than 50%, which is acceptable for practical mobile communication applications and will be discussed later with the aid of Figure 13.

Effects of the capacitive feeding branch are analyzed with the aid of Figure 5. Results of the simulated return loss for the proposed antenna, the case without the inductive feeding branch and matching network (Ant3), and the case without the inductive feeding branch (Ant4) are shown. In this case, it is seen that there is no resonant mode generated in the desired lower band for Ant3 and Ant4. This suggests that the desired lower band cannot be generated when the inductive feeding branch is not present. Also note that for Ant3, a resonant mode is generated at about 2 GHz, which however cannot cover the desired higher band. By adding the matching network to form Ant4, dual-resonance excitation is obtained, and the bandwidth can cover the 1710–2690 MHz band.

Effects of the matching network on both the lower and higher bands are discussed with the aid of Figure 6, in which the simulated return loss for the proposed antenna and the case without the matching network (Ant5) are shown. It is seen that the matching network can cause dual-resonance excitation in both the lower and higher bands to, respectively, cover the desired 698–960 and 1701–2690 MHz bands. To show the effects of the matching network, the simulated input impedance on the Smith chart for Ant5 (curve 1), Ant5 with L_1, C_1, C_2 (curve 2), and Ant5 with L_1, C_1, C_2, L_2 (curve 3, proposed antenna) are shown in Figure 7. The first three elements (shunt inductor L_1, shunt capacitor C_1, and series capacitor C_2) are used to achieve dual-resonance for the excited resonant mode in
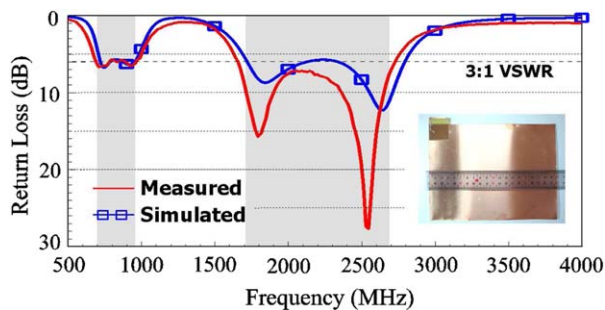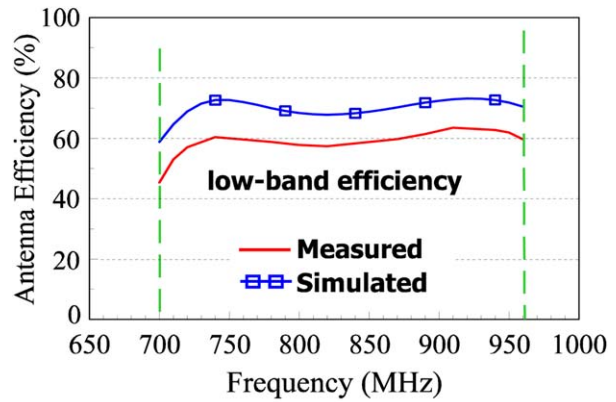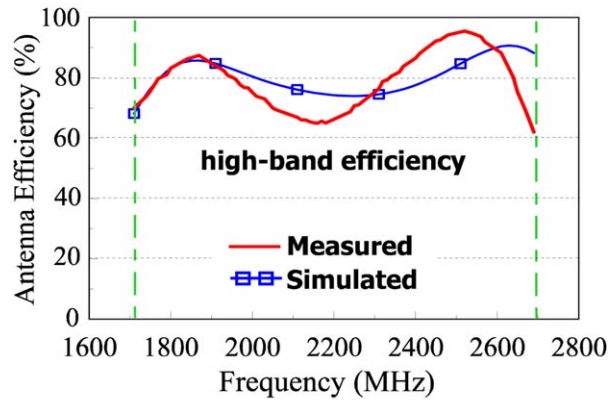

Figure 12 Measured and simulated return loss of the fabricated antenna. [Color figure can be viewed in the online issue, which is available at wileyonlinelibrary.com]

(a)

(b)

Figure 13 Measured and simulated antenna efficiency of the fabricated antenna. (a) Low band. (b) High band. [Color figure can be viewed in the online issue, which is available at wileyonlinelibrary.com]

the lower band. As seen in Figure 7(a), a dual-resonance impedance matching is obtained (see curve 1 vs. curve 2). By further adding the series inductor L_2, the dual-resonance impedance curve is shifted into the 3:1 VSWR circle (see curve 2 vs. curve 3). For the higher band, it is seen in Figure 7(b) that the first three elements (L_1, C_1, C_2) make the high-band impedance curve more capacitive (see curve 1 vs. curve 2). Hence, with the series inductor L_2 added, the high-band impedance matching improves, and the impedance curve is also shifted into the 3:1 VSWR circle with a dual-resonance behavior (see curve 2 vs. curve 3).

The simulated surface current distributions of the proposed antenna are also shown in Figure 8. The results clearly indicate that in the lower band, the antenna is mainly excited through the inductive feeding branch (see the results at 750 MHz). Although in the higher band, the antenna is mainly excited through the capacitive feeding branch (see the results at 2500 MHz). These results also confirm that the antenna's lower and higher bands are, respectively, owing to the inductive and capacitive feeding branches.

3.3. Parametric Study
A parametric study on the loaded chip inductor and capacitor in the two feeding branches is also conducted. Figure 9 shows the simulated return loss as a function of the inductance L in the inductive feeding branch. Results for $L = 4$, 7, and 10 nH are shown. Results for the case with a simple feeding strip (no chip inductor loaded) replacing the inductive feeding branch are also
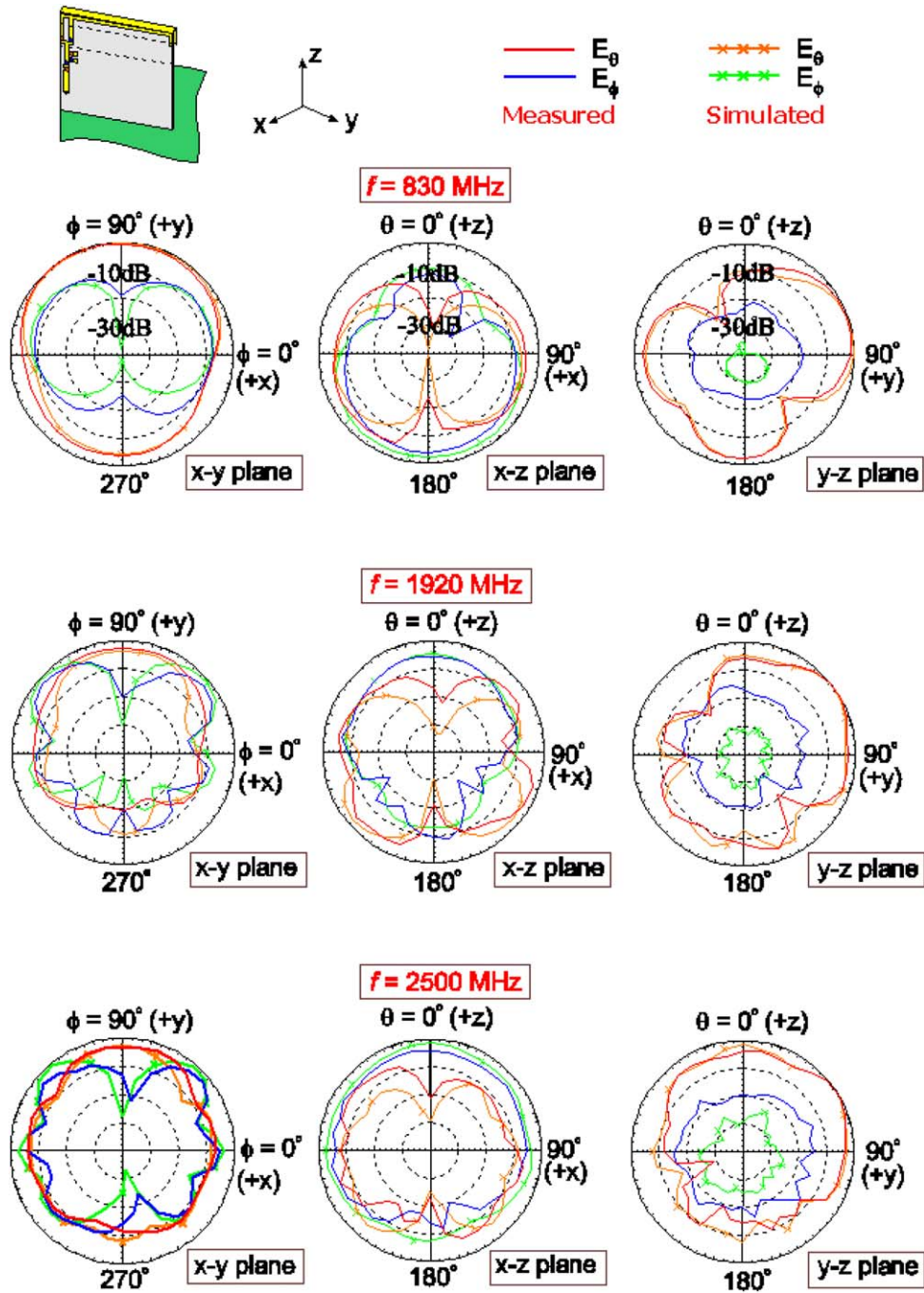
Figure 14 Measured and simulated radiation patterns of the fabricated antenna. [Color figure can be viewed in the online issue, which is available at wileyonlinelibrary.com]

presented. When there is no inductor loaded, large effects on both the lower and higher bands are seen. Conversely, for $L = 4$, 7, and 10 nH, small effects on the higher band are seen. With increasing inductance, the excited resonant mode owing to the inductive feeding branch is seen to occur at decreasing frequencies. Results indicate that the loaded inductor in the inductive feeding branch not only controls the antenna's lower band but also causes good isolation between the two feeding branches.

Figure 10 shows the simulated return loss as a function of the capacitance C in the capacitive feeding branch. Results for $C = 0.8$, 1.0, and 1.2 pF are shown. Results for the case of using a simple feeding strip instead of using the capacitive feeding branch are also shown for comparison. When a simple feeding

strip is used, large effects on both the lower and higher band are seen, similar to that observed in Figure 9. It is also seen that the variations in the capacitance not only cause some variations in the higher band but also have some effects on the lower band. This is mainly because the capacitance C is parallel to the inductive feeding branch, and the combined reactance of the parallel capacitance C and parallel inductance L in this study will be inductive and also larger than the inductance L for frequencies in the lower band. Hence, it is seen that with increasing capacitance C, the resonant mode in the lower band is shifted to lower frequencies. Owing to this additional effect of the capacitance C in lowering the resonant mode for the lower band, a smaller value of the inductance L loaded in the

inductive feeding branch can be applied ($L = 7$ nH in the proposed design).

Effects of the L-shaped metal plate are also studied with the aid of Figure 11, in which the simulated return loss for the proposed antenna and the case with a planar metal plate (Ant6) are presented. Results indicate that with the added L-shaped metal plate, larger bandwidths of the antenna's lower and higher bands can be obtained. Also note that with the presence of the L-shaped metal plate, the thickness of the antenna is increased to be 3 mm only, which makes the antenna still promising for applications in the modern slim tablet computer.

4. EXPERIMENTAL RESULTS AND DISCUSSION

Figure 12 shows the measured and simulated return loss of the fabricated antenna with the device ground plane. The antenna dimensions are given in Figure 1, and the device ground plane of size 150×200 mm^2 is cut from a 0.2-mm thick copper plate. The antenna is fed through a 50-Ω SMA connector placed at the back of the device ground plane and connected through a via to the antenna port (point A$'$ in Fig. 1). The measured return loss in general agrees with the simulated results. Over the 698–960 and 1710–2690 MHz bands, the measured return loss is better than about 3:1 VSWR (6 dB).

Figure 13 shows the measured and simulated antenna efficiency of the fabricated antenna. The antenna efficiency includes the mismatching loss and is measured in a far-field anechoic chamber. In the lower and higher bands, the measured antenna efficiency is, respectively, about 45–62 and 61–95%, which is acceptable for practical applications in mobile devices. The discrepancy between the measured and simulated results seen in the lower band is largely owing to the ohmic loss of the lumped elements in the proposed design. Although in the higher band, the lumped elements may also cause ohmic loss to decrease the antenna efficiency. However, as the measured return loss is generally better than the simulated return loss (see Fig. 12), the measured antenna efficiency is close to the simulated antenna efficiency in the higher band.

Figure 14 shows the measured and simulated radiation patterns of the fabricated antenna. Radiation patterns of three representative frequencies at 830, 1920, and 2500 MHz are presented. At each frequency, results for three principal planes are shown, and the patterns in the three planes are normalized with respect to the same maximum radiation intensity. The measured radiation patterns in general agree with the simulation results. In the y-z plane (elevation plane parallel to the device ground plane), asymmetric radiation patterns with respect to the z-axis are seen, which is mainly because the antenna is mounted at one corner of the top edge of the device ground plane. In the x-y plane (azimuthal plane), stronger radiation in the $+y$ direction than in the $-y$ direction is seen, which is again owing to the antenna mounted asymmetrically along the top edge of the device ground plane. In the x-z plane (elevation plane orthogonal to the device ground plane), it is seen that the radiation is stronger in the $-z$ direction at 830 MHz, while the radiation is stronger in the $+z$ direction at 2500 MHz. This is largely because the device ground plane also functions like a radiator at lower frequencies. However, at higher frequencies, the device ground plane behaviors more like a reflector, thus causing stronger radiation in the upper half hemisphere in the x-z plane.

5. CONCLUSION

A simple monopole antenna with an inductive feeding branch and a capacitive feeding branch for the LTE/WWAN operation

in the tablet computer has been proposed. The simple monopole antenna can provide two operating bands, with the lower one owing to the inductive feeding branch and the higher one owing to the capacitive feeding branch. The two operating bands are easy to control and the bandwidths, therefore, can be enhanced to cover the desired 698–960 and 1710–2690 MHz by a simple matching network. For applications in the tablet computer, the antenna requires a small clearance region of 10×30 mm^2 above the top edge of the device ground plane. The operating principle of the proposed antenna has been described. Good radiation characteristics have been obtained for the antenna. In addition to the small ground clearance required, the antenna shows a thin thickness of 3 mm, which makes it promising for modern slim tablet computer applications.

REFERENCES

1. J.S. lee, H. Rhyu, and B. Lee, Design concept of multi-band antenna with resonant circuit on PCB, Electron Lett 43 (2007), 315–317.
2. R. Valkonen, J. Ilvonen, C. Icheln, and P. Vainikainen, Inherently non-resonant multi-band mobile terminal antenna, Electron Lett 49 (2013), 11–13.
3. R. Valkonen, M. Kaltiokallio, and C. Icheln, Capacitive coupling element antennas for multi-standard mobile handsets, IEEE Trans Antennas Propag 61 (2013), 2783–2791.
4. K.L. Wong and L.Y. Chen, Small-size LTE/WWAN tablet device antenna with two hybrid feeds, IEEE Trans Antennas Propag 62 (2014), 2926–2934.
5. K.L. Wong, Planar antennas for wireless communications, Wiley, New York, 2003.
6. K.L. Wong and T.W. Weng, Small-size triple-wideband LTE/WWAN tablet device antenna, IEEE Antennas Wireless Propag Lett 12 (2013), 1516–1519.
7. K.L. Wong, H.J. Jiang, and T.W. Weng, Small-size planar LTE/WWAN antenna and antenna array formed by the same for tablet computer application, Microwave Opt Technol Lett 55 (2013), 1928–1934.
8. J.H. Lu and Y.S. Wang, Internal uniplanar antenna for LTE/GSM/UMTS operation in a tablet computer, IEEE Trans Antennas Propag 61 (2013), 2841–2846.
9. J.H. Lu and F.C. Tsai, Planar internal LTE/WWAN monopole antenna for tablet computer application, IEEE Trans Antennas Propag 61 (2013), 4358–4363.
10. Y.L. Ban, S.C. Sun, J.L.W. Li, and W. Hu, Compact coupled-fed wideband antenna for internal eight-band LTE/WWAN tablet computer applications, J Electromagn Waves Appl 26 (2012), 2222–2233.
11. K.L. Wong and W.J. Lin, WWAN/LTE printed slot antenna for tablet computer application, Microwave Opt Technol Lett 54 (2012), 44–49.
12. K.L. Wong, Y.C. Liu, and L.C. Chou, Bandwidth enhancement of WWAN/LTE tablet computer antenna using embedded parallel resonant circuit, Microwave Opt Technol Lett 54 (2012), 305–309.
13. K.L. Wong and T.J. Wu, Small-size LTE/WWAN coupled-fed loop antenna with band-stop matching circuit for tablet computer, Microwave Opt Technol Lett 54 (2012), 1189–1193.
14. S.H. Chang and W.J. Liao, A broadband LTE/WWAN antenna design for tablet PC, IEEE Trans Antennas Propag 60 (2012), 4354–4359.
15. K.L. Wong and M.T. Chen, Small-size LTE/WWAN printed loop antenna with an inductively coupled branch strip for bandwidth enhancement in the tablet computer, IEEE Trans Antennas Propag 61 (2013), 6144–6151.
16. W.S. Chen and W.C. Jhang, A planar WWAN/LTE antenna for portable devices, IEEE Antennas Wireless Propag Lett 12 (2013), 19–22.
17. K.L. Wong and S.C. Chen, Printed single-strip monopole using a chip inductor for penta-band WWAN operation in the mobile phone, IEEE Trans Antennas Propag 58 (2010), 1011–1014.

18. K.L. Wong, 4G/multiband handheld device ground antennas, In: 2013 Asia-Pacific Microwave Conference Proceedings, Seoul, Korea, pp. 134–136.

19. P.W. Lin and K.L. Wong, Dual-feed small-size LTE/WWAN strip monopole antenna for tablet computer applications, Microwave Opt Technol Lett 55 (2013), 2571–2576.

20. M. Tzortzakakis and R. Langley, Quad-band internal mobile phone antenna, IEEE Trans Antennas Propag 55 (2007), 2097–2103.

21. Z. Zhang, J.-C. Langer, K. Li, and M.F. Iskander, Design of ultrawideband mobile phone stubby antenna (824 MHz-6 GHz), IEEE Trans Antennas Propag 56 (2008), 2107–2111.

22. Available at: http://www.ansys.com/products/ ANSYS HFSS, Ansoft Corp., Pittsburgh, PA.

Figure 1 (a) The I-V curve of ATF-38143 and (b) the biasing network used in the proposed PA. [Color figure can be viewed in the online issue, which is available at wileyonlinelibrary.com]

DESIGN OF X-BAND POWER AMPLIFIER FOR LEO SATELLITE TRANSMITTER

Islam Mansour,[1] **Hadia Elhennawy,**[2] **and Adly S. Tag El-Dien**[1]
[1] Department of Electronics and Communication, Shoubra Faculty of Engineering, Banha University, Cairo, Egypt; Corresponding author: eng_islam_mansour@yahoo.com
[2] Department of Electronics and Communication Engineering, Ain Shams University, Cairo, Egypt

ABSTRACT: *The design of a three-stage X-band power amplifier (PA) is presented in this article. The amplifier is realized using an ATF-38143 low noise PHEMT FET. The proposed PA achieves 17–18.3 dB power gain, a good input matching ($S_{11} < -8$ dB) and a good output matching ($S_{22} < -10$ dB). The average power added efficiency when the input power 5 dBm is 50% over the 4-GHz bandwidth (from 8 to 12 GHz). The total power consumption of the PA is 0.24 W from 2.5 V supply voltage. Its performance was simulated using Agilent EEs of ADS simulator. The PA is fabricated with photolithographic technique and scattering parameters are measured using Agilent Vector Network Analyzer ES1978. Measurements and simulations show good agreement. © 2015 Wiley Periodicals, Inc. Microwave Opt Technol Lett 57:860–865, 2015; View this article online at wileyonlinelibrary.com. DOI 10.1002/mop.28979*

Key words: *low earth orbit; X-band; power amplifiers; PHEMT; inductive degeneration; LPF*

1. INTRODUCTION

Modern satellite communication systems require high data rate, high-efficiency, and simple transmitters, without sacrificing linearity depending on the modulation scheme. Low earth orbit (LEO) satellites dedicated for earth remote sensing applications, especially those concerned with land imaging, use high bit rates for image data downloading to the ground stations. Such satellites usually operate in the X-band of the microwave frequency spectrum. According to the excessive noise at such relatively high frequency and the wideband of operation; it becomes an essential requirement to transmit the data through a high microwave power to the ground stations. Power amplifiers (PA) are among the most important elements in transmission system chains. Optimizing efficiency, linearity, output power, and bandwidth remains a challenging task for the designer although several different design techniques and circuit solutions are available [1]. After PA; LPF is used to eliminate the harmonics generated from the PA and transmitting only the required signal.

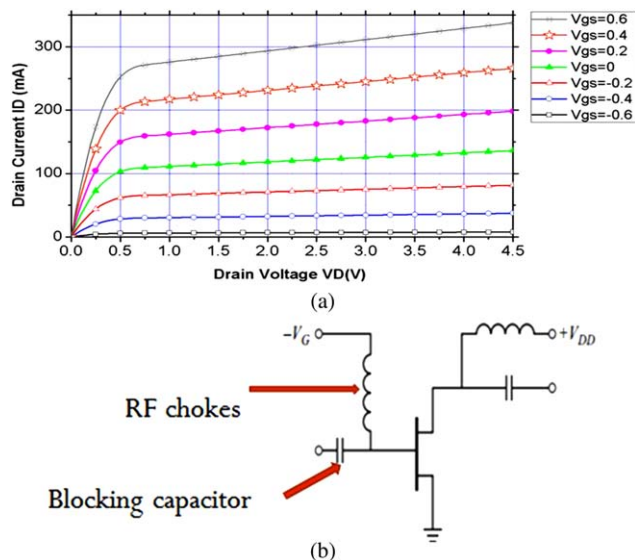The proposed PA is consisted of a three stage common source (CS) amplifier to achieve optimum output power and gain while maintaining a wide bandwidth; the wide bandwidth is achieved by inductive degeneration technique. The proposed PA in this article is simulated using ADS 2009. The PA is fabricated using thin film photolithographic technique. The scattering parameters are measured using vector network analyzer ES1978A. The power measurements are made using spectrum analyzer. The PA is fabricated on Rogers RT5880 substrate with thickness of 1.575 mm, relative permittivity of 2.2 and tan δ = 0.0009.

In Section 2, the PA design concept is illustrated. The proposed PA is presented in Section 3. Measured and simulated results are presented in Section 4. While, the article conclusion is given in Section 5.

2. PA DESIGN CONCEPT

2.1. Transistor Selection
The first step in the design of any amplifier is choosing the suitable transistor. There are two types of transistor bipolar junction transistor (BJT) and FET. BJT is current controlled but FET is voltage controlled. FET amplifiers have greater bandwidth than equivalent BJT topologies. FET amplifier has a smaller voltage gain than BJT. In the proposed PA, design ATF-38143 is used which is high dynamic range, low noise, high IP3, low cost, PHEMT housed in a 4-lead surface mount plastic package and suitable for LEO systems [3].

2.2. Biasing Circuit
After choosing the transistor it is required to estimate the *I-V* characteristic. To estimate the *I-V* curve it is required to build up the circuit shown in Figure 1(a), the gate source voltage is swept from -0.6 V to 0.6 V and the drain source voltage is swept from 0 V to 4.5 V as mentioned in datasheet. The *I-V* curve of ATF-38143 is shown in Figure 1(b). Choosing the suitable Q-point depends on the application (low noise, high gain, high power), the class of the amplifier (class A, class AB, class B), and the transistor. The maximum allowed DC power dissipation of ATF-38143 is equal to 0.58 watts. This value will limit the choice of the bias level to ensure a secure operation region for the transistor.